Proc. Natl. Acad. Sci. USA
Vol. 91, pp. 9332–9336, September 1994
Biochemistry

Ligand-induced formation of nucleic acid triple helices

(triplex induction/triplex drug binding/RNA–DNA hybrid duplexes and triplexes/Hoogsteen melting transitions/antigene)

DANIEL S. PILCH AND KENNETH J. BRESLAUER*

Department of Chemistry, Rutgers-The State University of New Jersey, New Brunswick, NJ 08903

Communicated by Richard E. Dickerson, May 17, 1994

ABSTRACT **We demonstrate that ligand binding can be used to induce the formation of triplex structures that would not otherwise form. Specifically, we show that binding of berenil or 4′,6-diamidino-2-phenylindole (DAPI) induces formation of the poly(rA)·poly(rA)·poly(dT) triplex, providing an example of an RNA(purine)·RNA(purine)·DNA(pyrimidine) triplex. We also show that binding of berenil, DAPI, ethidium, or netropsin can induce formation of the poly(dT)·poly(rA)·poly(dT) triplex, thereby overcoming a practical limitation to the formation of DNA·RNA·DNA triplexes with a purine RNA strand. Based on the enhanced thermal stabilities of the drug-bound poly(dT)·poly(rA)·poly(dT) complexes at 18 mM Na^+, we define the relative triplex-inducing efficiencies of these four ligands to be: berenil > DAPI > ethidium > netropsin. Our results demonstrate that ligand binding can be used to induce the formation of triplex structures that do not form in the absence of the ligand. This triplex-inducing capacity has potentially important implications in the design of novel antisense, antigene, and diagnostic strategies.**

Nucleic acid triple helices currently are the focus of considerable attention. This attention in large part is due to the potential biomedical applications of triplex structures (1–8), which include the specific control of cellular processes, such as transcription and replication, and the mapping of megabase DNA through the selective cleavage of specific DNA duplex domains (9, 10). The effective development of such applications of triple helices requires a data base that allows one to predict and/or control the relative affinities and specificities of third-strand probes for target DNA·DNA, RNA·RNA, and RNA·DNA duplex domains, and to predict the relative stabilities of the resulting triplex structures. In recognition of this need, several major systematic studies have appeared which elucidate the influence of "strand composition" (RNA versus DNA) on the stabilities and energetic properties of intermolecular triplex structures (11–14). The overall data base provided by these studies contains comparatively little information about triplexes containing purine third strands [e.g., RNA(purine)·RNA(purine)·DNA(pyrimidine)] compared with those containing pyrimidine third strands. Significantly, these studies find that triplex formation favors RNA in both pyrimidine strands and DNA in the purine strand, with no report of either a DNA(pyrimidine)·RNA(purine)·DNA(pyrimidine) triplex or an RNA(purine)·RNA(purine)·DNA(pyrimidine) triplex.

In this paper, we demonstrate that a range of nucleic acid-binding ligands can, in fact, *induce* formation of two classes of intermolecular triple helices which do not form in the absence of ligand binding—namely, a DNA(pyrimidine)·RNA(purine)·DNA(pyrimidine) triplex and an RNA(purine)·RNA(purine)·DNA(pyrimidine) triplex. In this connection, several previous studies have used nucleic acid-binding ligands as part of efforts to modulate the properties of triplex structures (15–23). However, those studies only assessed the impact of ligand binding on the properties of *preformed* triplexes. This report provides an example of the use of ligand binding to induce formation of triple helices that would otherwise not form. The ability of ligands to alter dramatically the affinity and specificity of third strands for their double-helical targets opens the door to the design of novel antisense, antigene, and diagnostic strategies.

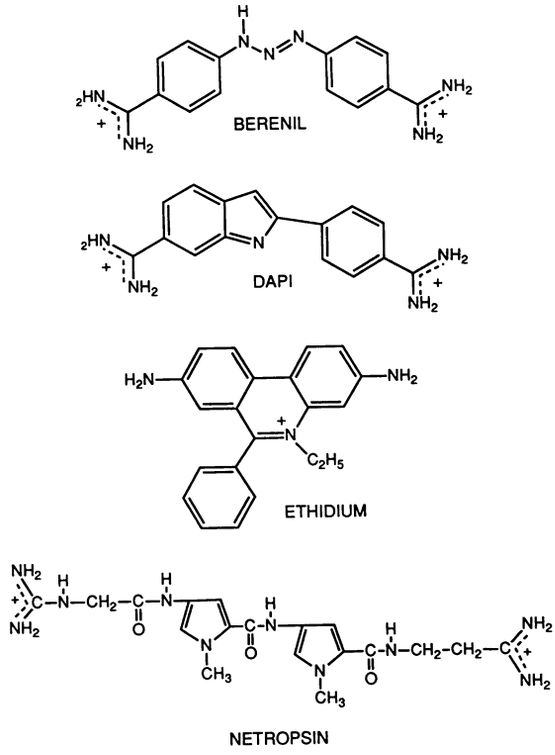

FIG. 1. Structures of berenil, DAPI, Etd, and netropsin.

To evaluate the influence of nucleic acid-binding ligands on intermolecular triplexes, we have studied the effects of berenil [1,3-*bis*(4′-amidinophenyl)triazene], 4′,6-diamidino-2-phenylindole (DAPI), ethidium bromide (EtdBr), and netropsin (Fig. 1) on the formation of the poly(dT)·poly(rA)·poly(dT) triplex [abbreviated (dT)·(rA)·(dT)] and the poly(rA)·poly(rA)·poly(dT) triplex [abbreviated (rA)·(rA)·(dT)]. These four ligands were selected because they encompass a wide range of nucleic acid-binding modes, with reasonably well-characterized nucleic acid-binding properties (refs. 24–39, 41, and 42; unpublished results).

The publication costs of this article were defrayed in part by page charge payment. This article must therefore be hereby marked "*advertisement*" in accordance with 18 U.S.C. §1734 solely to indicate this fact.

Abbreviations: (dT)·(rA)·(dT), poly(dT)·poly(rA)·poly(dT); (rA)·(rA)·(dT), poly(rA)·poly(rA)·poly(dT); HG, Hoogsteen; W-C, Watson–Crick; DAPI, 4′,6-diamidino-2-phenylindole; Etd, ethidium.

*To whom reprint requests should be addressed.

MATERIALS AND METHODS

Nucleic Acid Polymers and Ligand Molecules. Berenil, DAPI, and EtdBr were purchased from Sigma. Netropsin was obtained from Boehringer Mannheim. All ligands were of the highest grades commercially available and were used without further purification. Synthetic poly(rA) and poly(dT) were purchased from Pharmacia and also were used without further purification. Concentrations of ligand and polymer stock solutions were determined spectrophotometrically.

UV Mixing Curves. Stock solutions of poly(rA) and poly(dT) in either the absence or the presence of berenil (15 μM) were prepared at equal concentrations (30 μM nucleotide). Portions of each solution were mixed at the appropriate volumetric ratios and, after equilibration, the absorbance at 260 nm was measured. To construct the mixing curve at 390 nm, 1 ml of a 40 μM poly(dT) solution containing 20 μM berenil was added to a cuvette, followed by addition of portions (1.3–34 μl) of a 2 mM poly(rA) solution. After equilibration, the absorbance at 390 nm was measured.

UV Spectroscopy. UV melting curves at 260 nm were determined at a scan rate of 0.1°C/min with a Perkin–Elmer Lambda 4C spectrophotometer. The nucleic acid concentrations were 90 μM nucleotide (30 μM base triplet) and the ligand concentrations were 0, 15, or 30 μM.

CD Spectropolarimetry. CD melting curves were determined using an Aviv model 60DS spectropolarimeter (Aviv Associates, Lakewood, NJ). The nucleic acid concentrations were 120 μM nucleotide (40 μM base triplet) and the ligand concentrations were 0, 20, or 40 μM.

RESULTS AND DISCUSSION

Stoichiometry of the Complexes. To establish the stoichiometries of the complexes formed by mixing poly(rA) and poly(dT) strands in the absence and presence of ligand, we used the method of continuous fractions (43–46). Mixing curves were determined at 260 nm for poly(rA) and poly(dT) in the absence (Fig. 2*A*) or presence (Fig. 2*B*) of berenil.

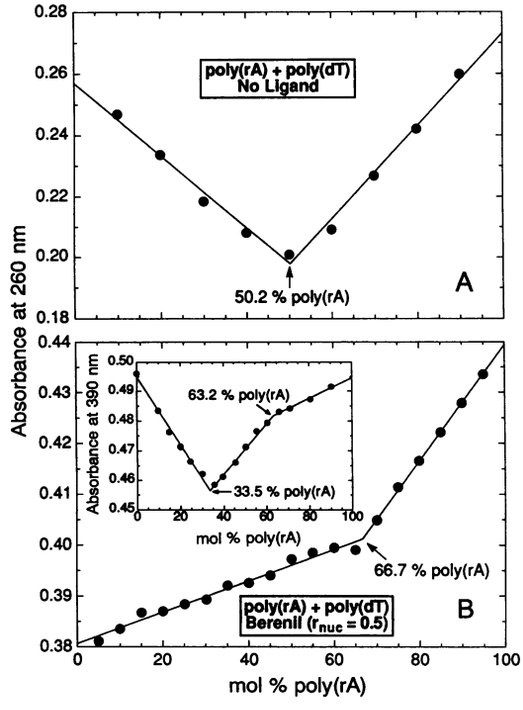

FIG. 2. Absorbance mixing curves at 260 nm showing the stoichiometry of complexes formed by poly(rA) and poly(dT) in the absence (*A*) and presence (*B*) of berenil {r_{nuc} = [total berenil]/[nucleotide]}. (*Inset*) Absorbance mixing curve at 390 nm showing the stoichiometry of complexes formed by poly(rA) and poly(dT) in the presence of berenil. Buffer conditions for all mixing curves were 10 mM sodium cacodylate, pH 7.0/8 mM NaCl/0.1 mM EDTA.

Berenil binding induces formation of the (dT)·(rA)·(dT) and (rA)·(rA)·(dT) triplexes, neither of which forms in the absence of the ligand. Inspection of the mixing curves in Fig. 2 reveals that in the absence of ligand, a single inflection point is observed at ≈50% poly(rA). This stoichiometry is consistent with the formation of the expected 1:1 poly(rA)/poly(dT) complex (44), which corresponds to the poly(rA)·poly(dT) duplex [abbreviated (rA)·(dT)]. Thus, in the absence of ligand, neither the (dT)·(rA)·(dT) nor the (rA)·(rA)·(dT) triplex forms under the solution conditions employed (18 mM Na^+, pH 7.0). However, inspection of Fig. 2*B* reveals that in the presence of berenil, a single inflection point is observed at 66.7% poly(rA), establishing the formation of a 2:1 poly(rA)/poly(dT) complex which corresponds to the (rA)·(rA)·(dT) triplex. Fig. 2*B Inset* shows another mixing curve in which the absorbance at 390 nm (where only berenil absorbs) also was used to monitor the stoichiometries of the complexes formed by mixing the poly(rA) and poly(dT) strands. At this wavelength the mixing curve has two inflection points rather than just one. As with the mixing curve at 260 nm, an inflection point occurs at 63.2% poly(rA), reaffirming formation of the 2:1 poly(rA)/poly(dT) complex which corresponds to the (rA)·(rA)·(dT) triplex. However, in the 390-nm mixing curve, a second inflection point, at 33.5% poly(rA), reflects the formation of a 1:2 poly(rA)/poly(dT) complex corresponding to the (dT)·(rA)·(dT) triplex, a structure undetected by the mixing curve at 260 nm. The mixing curves are consistent with berenil inducing formation of both the (rA)·(rA)·(dT) and (dT)·(rA)·(dT) triplexes and highlight the importance of using multiple wavelengths to monitor the stoichiometry of nucleic acid complexes, both in the absence and in the presence of ligands.

DAPI, EtdBr, and netropsin also induce formation of the (dT)·(rA)·(dT) triplex, but only DAPI and berenil induce formation of the (rA)·(rA)·(dT) triplex at 18 mM Na^+. The stoichiometries of the complexes formed at 18 mM Na^+ by the poly(rA) and poly(dT) strands in the presence of either DAPI, EtdBr, or netropsin also were obtained in a similar fashion (data not shown). These mixing curves reveal that—as with berenil—DAPI, EtdBr, and netropsin also induce formation of a complex corresponding to the (dT)·(rA)·(dT) triplex, but only DAPI and berenil induce formation of a complex corresponding to the (rA)·(rA)·(dT) triplex. This latter result is not surprising, since berenil and DAPI are structurally similar ligands (Fig. 1) and exhibit many similar nucleic acid-binding properties (refs. 34–39 41, and 42; unpublished results). In summary, in the presence of the appropriate ligand, poly(rA) and poly(dT) strands can be induced to form the (dT)·(rA)·(dT) triplex and/or the (rA)·(rA)·(dT) triplex, neither of which forms in the absence of ligand.

Thermally Induced Denaturation of the Complexes as Measured by UV Absorbance. We used temperature-dependent UV absorbance measurements at 260 nm to monitor the thermally induced denaturation of the complexes formed by poly(rA) and poly(dT) in the absence and presence of ligand. Illustrative melting curves with berenil as the ligand are shown in Fig. 3.

In the absence of berenil, only the (rA)·(dT) duplex → single strand transition is observed for both the 1:2 poly(rA)/poly(dT) and 2:1 poly(rA)/poly(dT) solutions. In the absence of ligand, solutions containing either a 1:2 or a 2:1 stoichiometry of poly(rA) and poly(dT) strands (Fig. 3 *A* and *C*, respectively) each exhibit a single Watson–Crick (W-C) transition (T_{max} = 49.9°C) which corresponds to the well-known denaturation of the (rA)·(dT) duplex (44). These melting-curve results in the absence of ligand are consistent with the

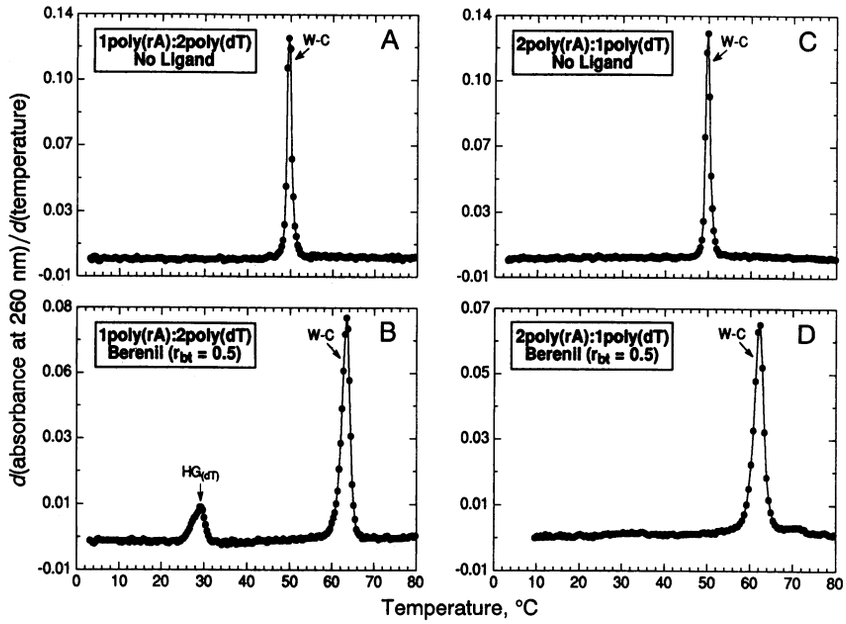

FIG. 3. Derivatives of absorbance melting profiles at 260 nm of solutions with stoichiometric poly(rA)/poly(dT) ratios of either 1:2 (*A* and *B*) or 2:1 (*C* and *D*). The melting curves in *A* and *C* are in the absence of berenil, while those in *B* and *D* are in the presence of berenil. Buffer conditions were identical to those described in the legend of Fig. 2. The designation $HG_{(dT)}$ corresponds to the Hoogsteen transition in which the poly(dT) third strand dissociates from the poly(rA)·poly(dT) duplex. W-C refers to the Watson–Crick transition corresponding to dissociation of the poly(rA)·poly(dT) duplex. r_{bt} = [total berenil]/[base triplet].

corresponding mixing curve (Fig. 2*A*), which also reveals that in the absence of ligand neither the (dT)·(rA)·(dT) nor the (rA)·(rA)·(dT) triplex is formed under the solution conditions employed (18 mM Na^+, pH 7.0). In other words, the second equivalent of either the poly(dT) or the poly(rA) strand remains as an unhybridized single strand. Chamberlin and coworkers (44) found that the (dT)·(rA)·(dT) triplex could be formed only under extreme solution conditions (2.5 M Na^+), in contrast to the mild conditions (18 mM Na^+) under which we show ligand binding-induced formation of the same triplex. Our observation that, in the absence of ligand, single-stranded poly(dT) does not hybridize with the (rA)·(dT) duplex to form the (dT)·(rA)·(dT) triplex agrees with the independent findings of the Crothers, Dervan, and Hélène groups (11, 12, 14), who have shown that a pyrimidine DNA third strand will not bind to a hybrid duplex containing a purine RNA strand. Our results also reveal that, in the absence of ligand, a purine RNA third strand [in this case, poly(rA)] will not bind a hybrid duplex containing a purine RNA strand [in this case, poly(rA)·poly(dT)], even though a pyrimidine RNA strand has been shown to bind, albeit weakly, to such a hybrid duplex (11, 12). Since purine RNA strands have been shown to bind duplexes with RNA in both strands (47, 48), our results may reflect conformational/energetic differences between hybrid RNA·DNA duplexes and the corresponding all-RNA duplexes.

In the presence of berenil, two melting transitions are observed for the 1:2 poly(rA)/poly(dT) solution: the (dT)·(rA)·(dT) triplex → (rA)·(dT) duplex transition followed by the (rA)·(dT) duplex → single strand transition. In striking contrast to the single transition in the melting profile of a 1:2 poly(rA)/poly(dT) solution in the absence of berenil (Fig. 3*A*), we observe two transitions in the melting profile in the presence of berenil (Fig. 3*B*). One of these transitions (T_{max} = 63.4°C) corresponds to the expected W-C transition. We assign the second berenil-induced transition (T_{max} = 29.0°C) to the dissociation of poly(dT) from the (rA)·(dT) duplex [the $HG_{(dT)}$ transition]. This assignment is consistent with the mixing curve results shown in Fig. 2*B Inset*, which reveal that berenil binding induces formation of the (dT)·(rA)·(dT) triplex. Thus, for the 1:2 poly(rA)/poly(dT) solution in the presence of berenil, the mixing curves and the melting profiles are consistent in revealing the presence of two complexes.

In the presence of berenil, only one melting transition is observed for the 2:1 poly(rA)/poly(dT) solution: the (rA)·(dT) duplex → single strand transition. By contrast to the melting behavior noted above for the 1:2 poly(rA)/poly(dT) solution in the presence of berenil, the melting behavior of the 2:1 poly(rA)/poly(dT) solution at 260 nm (Fig. 3*D*) and other wavelengths in the presence of berenil reveals only a single transition, which corresponds to the thermally induced disruption of just one of the two complexes defined by the mixing curves. More specifically, for the 2:1 poly(rA)/poly(dT) solution in the presence of berenil, only the W-C transition (T_{max} = 62.3°C) is observed, making the melting profile similar to that associated with the identical solution in the absence of berenil (Fig. 3*C*), with the exception of the expected berenil-induced increase in duplex thermal stability. Consequently, this melting profile (Fig. 3*D*) appears to be inconsistent with the mixing curves of Fig. 2*B*, which reveal that berenil binding also induces formation of the (rA)·(rA)·(dT) triplex. However, this apparent inconsistency simply reflects the different distribution of states in an isothermal mixing experiment (Fig. 2*B*) versus a melting experiment (Fig. 3*D*), as well as different absorbance ranges over which the two experiments were performed. Below we demonstrate experimentally that this apparent inconsistency is not real but rather simply reflects the fact that temperature-dependent UV absorbance curves can be blind to some triplex melting transitions which can be detected by other temperature-dependent optical techniques, thereby underscoring the need to use multiple spectroscopic methods for detecting and characterizing nucleic acid triplex transitions.

Thermally Induced Denaturation of the Complexes as Measured by CD Spectropolarimetry. To address the apparent inconsistency noted above, we also used temperature-dependent CD spectropolarimetry at various wavelengths to investigate the melting of the complexes formed by the poly(rA) and poly(dT) strands in the absence and presence of ligand. Illustrative CD melting profiles are shown in Fig. 4.

Detection of both melting transitions depends on the observable employed and the wavelength monitored. In the absence of ligand, the CD melting curve of a 1:2 poly(rA)/poly(dT) solution shows a single W-C transition (Fig. 4*A*), while in the presence of berenil (r_{bt} = 0.5) the CD profile exhibits two transitions (Fig. 4 *B* and *C*). As observed in the absorbance melting profile (Fig. 3*B*) and discussed above, these CD-detected transitions correspond to either the W-C or the $HG_{(dT)}$ dissociation reactions, thereby reaffirming that berenil binding induces formation of the (dT)·(rA)·(dT) tri-

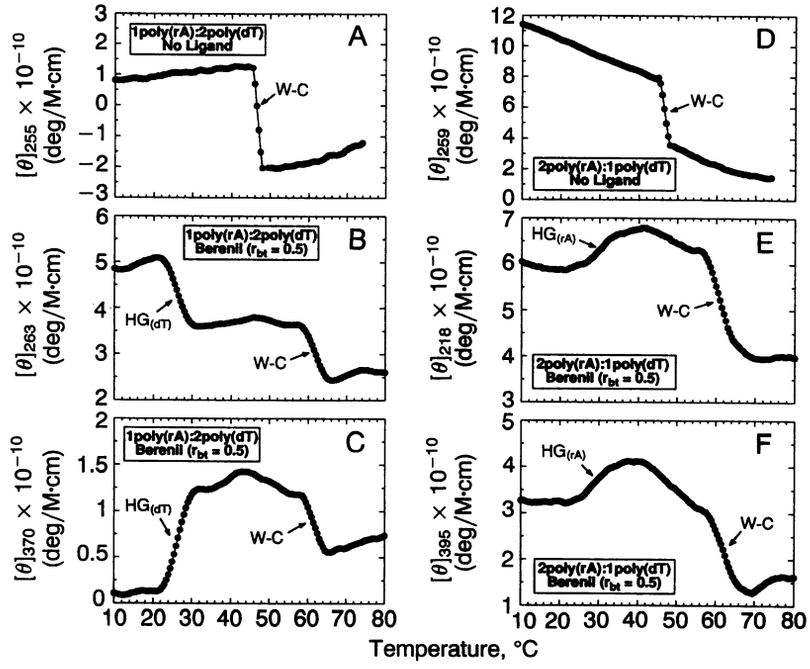

FIG. 4. CD melting profiles at the indicated wavelengths of solutions with stoichiometric poly(rA)/poly(dT) ratios of either 1:2 (*A–C*) or 2:1 (*D–F*). The melting curves in *A* and *D* are in the absence of berenil, while those in *B*, *C*, *E*, and *F* are in the presence of berenil. In a typical experiment, the temperature was raised in 0.5°C increments with a 1-min equilibration time at each temperature setting. Buffer conditions were identical to those described in the legend of Fig. 2. All molar ellipticities ([θ]) are in units of degrees (mol of base triplet/liter)$^{-1}$cm^{-1}. The designations $HG_{(dT)}$, W-C, and r_{bt} are as described in the legend of Fig. 3. $HG_{(rA)}$ corresponds to the Hoogsteen transition for the (rA)·(rA)·(dT) triplex.

plex. The greatest change in ellipticity associated with the $HG_{(dT)}$ transition occurs at 272 nm, the wavelength at which free single-stranded poly(dT) has a large CD signal (data not shown). This observation is consistent with dissociation of the poly(dT) third strand from the (rA)·(dT) duplex.

In the absence of berenil, the CD melting profiles of a 2:1 poly(rA)/poly(dT) solution at 259 nm (Fig. 4*D*) and 218 nm (data not shown) show single W-C transitions, as was observed for the absorbance melting profile (Fig. 3*C*). However, in marked contrast to the monophasic absorbance melting profile observed in the presence of berenil (Fig. 3*D*), the CD melting profiles at either 218 (Fig. 4*E*) or 395 (Fig. 4*F*) nm reveal two transitions. One transition (T_{min} = 61.0°C) corresponds to the expected W-C dissociation reaction, whereas the other transition (T_{max} = 29.8°C) reflects dissociation of the poly(rA) third strand from the (rA)·(dT) duplex [the $HG_{(rA)}$ transition]. Thus, although the absorbance melting curves at r_{bt} = 0.5 did not detect this, CD melting profiles reveal that berenil binding induces formation of the (rA)·(rA)·(dT) triplex, consistent with the results of the mixing curves in Fig. 2*B*. At wavelengths below 300 nm, we found the largest change in ellipticity associated with the $HG_{(rA)}$ transition to occur at 218 nm (Fig. 4*E*). This wavelength corresponds to that at which free single-stranded poly(rA) exhibits a large CD signal (data not shown). As was noted above for the $HG_{(dT)}$ transition at 272 nm, this observation is consistent with dissociation of the poly(rA) third strand from the (rA)·(dT) duplex in the $HG_{(rA)}$ transition. In the aggregate, our studies demonstrate that CD melting profiles at different wavelengths can reveal transitions that are absent from standard absorbance melting curves, and that the number of complexes discerned from such melting curves can depend on the wavelength monitored. These results underscore the critical importance of using multiple spectroscopic techniques at different wavelengths to define the stoichiometries of ligand–nucleic acid complexes and to characterize the thermally induced transitions of these complexes.

Relative Triplex-Inducing Capacities of the Ligands. UV and CD thermal denaturation experiments similar to those determined with berenil (Figs. 3 and 4) also were conducted in the presence of DAPI, EtdBr, or netropsin (Table 1). Inspection of these data reveals a number of features worthy of emphasis. (*i*) At r_{bt} = 1 and 18 mM Na^+, all four ligands induce formation of the (dT)·(rA)·(dT) triplex. (*ii*) As measured by the thermal stabilities of the ligand–(dT)·(rA)·(dT) complexes, the relative effectiveness of each ligand in inducing formation of the (dT)·(rA)·(dT) triplex follows the hierarchy berenil (T_{max} = 34.3 ± 1.0°C) > DAPI (T_{max} = 28.0 ± 1.0°C) > EtdBr (T_{max} = 11.9 ± 1.0°C) > netropsin (T_{max} = 3.8 ± 1.0°C). (*iii*) While binding by all four ligands induces formation of the (dT)·(rA)·(dT) triplex, only berenil and DAPI binding induces formation of the (rA)·(rA)·(dT) triplex. (*iv*) As measured by the thermal stabilities of the ligand–(rA)·(rA)·(dT) complexes, the relative effectiveness of each ligand in inducing formation of the (rA)·(rA)·(dT)

Table 1. Thermal stabilities of ligand-induced nucleic acid triplexes at 18 mM Na^+

Ligand	(dT)·(rA)·(dT) $HG_{(dT)}$ transition temperature, °C	(rA)·(rA)·(dT) transition temperature, °C
Berenil	34.3 ± 1.0	39.5 ± 1.0*
DAPI	28.0 ± 1.0	69.6 ± 1.0†
Ethidium	11.9 ± 1.0	—
Netropsin	3.8 ± 1.0	—

¶Buffer conditions are identical to those described in the legend of Fig. 2. At higher Na^+ concentrations (>150 mM), the rank order in column 2 is preserved, except that the positions of berenil and DAPI are reversed. In all cases, the [base triplet]/[total ligand] ratio ($1/r_{bt}$) is 1. Transition temperatures correspond to either a maximum or a minimum in a melting curve; —, not detected. The designation $HG_{(dT)}$ is as described in the legend of Fig. 3.

*T_{max} for the $HG_{(rA)}$ transition as described in the legend of Fig. 4.

†T_{max} for the (rA)·(rA)·(dT) triplex → single strand transition.

triplex follows the order DAPI (T_{max} = 69.6 ± 1.0°C) > berenil (T_{max} = 39.5 ± 1.0°C) >> EtdBr, netropsin (not detected). (v) The observed ligand-induced formation of the (dT)·(rA)·(dT) triplex and the (rA)·(rA)·(dT) triplex depends on both r_{bt} and the Na^+ concentration (data not shown). In general, high r_{bt} ratios (>0.1) favor triplex formation. These observations suggest that the mode of ligand binding, the strand composition of the third strand and the target duplex, the structural/conformational nature of the ligand–nucleic acid complex, and electrostatic interactions all influence ligand-induced formation of triple helices. To assess whether the charged ligands simply are exerting their electrostatic influence via an nonspecific counterion effect, we evaluated whether high Na^+ concentrations (up to 1 M) alone could induce triplex formation. These studies reveal that in the absence of ligand, high Na^+ concentrations alone are not sufficient to promote triplex formation, thereby indicating that specific ligand–nucleic acid interactions play key roles in triplex induction.

Concluding Remarks. In this report, we have demonstrated that drug binding can induce the formation of nucleic acid triplexes that otherwise would not form. Specifically, we have shown that berenil, DAPI, EtdBr, and/or netropsin can induce formation of a DNA(pyrimidine)·RNA(purine)·DNA(pyrimidine) triple helix and that berenil and DAPI can induce formation of an RNA(purine)·RNA(purine)·DNA(pyrimidine) triple helix. Thus, ligand binding can be used to overcome energetic barriers to the formation of specific triplex structures. Ligand-induced formation of new classes of hybrid triplexes potentially has important implications in the recognition of RNA·DNA duplexes by cellular and viral proteins. RNA·DNA hybrid duplexes are the primary targets for important enzymes such as ribonuclease H (49, 50) and reverse transcriptase (51). Triplex formation at enzyme recognition sites may provide a means for specific control of enzymatic function. Furthermore, by extension, the results reported here suggest that tethering suitable ligands to nucleic acid molecules with appropriate linkers (40, 52) may help reduce the stringency of conditions under which triplex formation occurs, as well as greatly reduce the effects of nonspecific ligand binding. In this way, novel antisense, antigene, and diagnostic strategies may be designed with greater degrees of specificity and efficacy.

This work was supported by National Institutes of Health Grants GM23509, GM34469, and CA47995.

1. Cooney, M., Czernuszewicz, G., Postel, E. H., Flint, S. J. & Hogan, M. E. (1988) *Science* **241**, 456–459.
2. Wells, R. D., Collier, D. A., Hanvey, J. C., Shimizu, M. & Wohlrab, F. (1988) *FASEB J.* **2**, 2939–2949.
3. Maher, L. J., III, Wold, B. & Dervan, P. B. (1989) *Science* **245**, 725–730.
4. Young, S. L., Krawczyk, S. H., Matteucci, M. D. & Toole, J. J. (1991) *Proc. Natl. Acad. Sci. USA* **88**, 10023–10026.
5. Hélène, C. (1991) *Anti-Cancer Drug Des.* **6**, 569–584.
6. Duval-Valentin, G., Thuong, N. T. & Hélène, C. (1992) *Proc. Natl. Acad. Sci. USA* **89**, 504–508.
7. Maher, L. J., III, Dervan, P. B. & Wold, B. (1992) *Biochemistry* **31**, 70–81.
8. Thuong, N. T. & Hélène, C. (1993) *Angew. Chem. Int. Ed. Engl.* **32**, 666–690.
9. Moser, H. E. & Dervan, P. B. (1987) *Science* **238**, 645–650.
10. Perrouault, L., Asseline, U., Rivalle, C., Thuong, N. T., Bisagni, E., Giovannangeli, C., Le Doan, T. & Hélène, C. (1990) *Nature (London)* **344**, 358–360.
11. Roberts, R. W. & Crothers, D. M. (1992) *Science* **258**, 1463–1466.
12. Han, H. & Dervan, P. B. (1993) *Proc. Natl. Acad. Sci. USA* **90**, 3806–3810.
13. Skoog, J. U. & Maher, L. J., III (1993) *Nucleic Acids Res.* **21**, 2131–2138.
14. Escudé, C., François, J.-C., Sun, J.-S., Ott, G., Sprinzl, M., Garestier, T. & Hélène, C. (1993) *Nucleic Acids Res.* **21**, 5547–5553.
15. Lehrman, E. & Crothers, D. M. (1977) *Nucleic Acids Res.* **4**, 1381–1392.
16. Bresloff, J. L. & Crothers, D. M. (1981) *Biochemistry* **20**, 3547–3553.
17. Mergny, J. L., Duval-Valentin, G., Nguyen, C. H., Perrouault, L., Faucon, B., Rougée, M., Montenay-Garestier, T. & Hélène, C. (1992) *Science* **256**, 1681–1684.
18. Pilch, D. S., Waring, M. J., Sun, J.-S., Rougée, M., Nguyen, C.-H., Bisagni, E., Garestier, T. & Hélène, C. (1993) *J. Mol. Biol.* **232**, 926–946.
19. Wilson, W. D., Tanious, F. A., Barton, H. J., Jones, R. L., Fox, K., Wydra, R. L. & Strekowski, L. (1993) *Biochemistry* **32**, 10614–10621.
20. Pilch, D. S., Martin, M.-T., Nguyen, C.-H., Sun, J.-S., Bisagni, E., Garestier, T. & Hélène, C. (1993) *J. Am. Chem. Soc.* **115**, 9942–9951.
21. Umemoto, U., Sarma, M. H., Gupta, G., Luo, J. & Sarma, R. H. (1990) *J. Am. Chem. Soc.* **112**, 4539–4545.
22. Park, Y.-W. & Breslauer, K. J. (1992) *Proc. Natl. Acad. Sci. USA* **89**, 6653–6657.
23. Durand, M., Thuong, N. T. & Maurizot, J. C. (1992) *J. Biol. Chem.* **267**, 24394–24399.
24. Waring, M. J. (1965) *J. Mol. Biol.* **13**, 269–282.
25. Crawford, L. V. & Waring, M. J. (1967) *J. Mol. Biol.* **25**, 23–30.
26. LePecq, J.-B. & Paoletti, C. (1967) *J. Mol. Biol.* **27**, 87–106.
27. Paoletti, J. & Le Pecq, J.-B. (1971) *J. Mol. Biol.* **59**, 43–62.
28. Nelson, J. W. & Tinoco, I., Jr. (1984) *Biopolymers* **23**, 213–233.
29. Waring, M. J. (1974) *Biochem. J.* **143**, 483–486.
30. Scaria, P. V. & Shafer, R. H. (1991) *J. Biol. Chem.* **266**, 5417–5423.
31. Mergny, J. L., Collier, D., Rougée, M., Montenay-Garestier, T. & Hélène, C. (1991) *Nucleic Acids Res.* **19**, 1521–1526.
32. Sun, J.-S., Lavery, R., Chomilier, J., Zakrzewska, K., Montenay-Garestier, T. & Hélène, C. (1991) *J. Biomol. Struct. Dyn.* **9**, 425–436.
33. Zimmer, C. & Wähnert, U. (1986) *Prog. Biophys. Mol. Biol.* **47**, 31–112.
34. Waring, M. J. (1970) *J. Mol. Biol.* **54**, 247–279.
35. Braithwaite, A. & Baguley, B. C. (1980) *Biochemistry* **19**, 1101–1106.
36. Portugal, J. & Waring, M. J. (1986) *Nucleic Acids Res.* **14**, 8735–8754.
37. Yoshida, M., Banville, D. L. & Shafer, R. H. (1990) *Biochemistry* **29**, 6585–6592.
38. Brown, D. G., Sanderson, M. R., Garman, E. & Neidle, S. (1992) *J. Mol. Biol.* **226**, 481–490.
39. Schmitz, H. U. & Hübner, W. (1993) *Biophys. Chem.* **48**, 61–74.
40. Giovannangeli, C., Montenay-Garestier, T., Rougée, M., Chassignol, M., Thuong, N. T. & Hélène, C. (1991) *J. Am. Chem. Soc.* **113**, 7775–7777.
41. Wilson, W. D., Tanious, F. A., Mizan, S., Yao, S., Kiselyov, A. S., Zon, G. & Strekowski, L. (1990) *Biochemistry* **29**, 8452–8461.
42. Tanious, F. A., Veal, J. M., Buczak, H., Ratmeyer, L. S. & Wilson, W. D. (1992) *Biochemistry* **31**, 3103–3112.
43. Job, P. (1928) *Ann. Chim. (Paris)* **9**, 113–134.
44. Riley, M., Maling, B. & Chamberlin, M. J. (1966) *J. Mol. Biol.* **20**, 359–389.
45. Pilch, D. S., Levenson, C. & Shafer, R. H. (1990) *Proc. Natl. Acad. Sci. USA* **87**, 1942–1946.
46. Plum, G. E., Park, Y.-W., Singleton, S. F., Dervan, P. B. & Breslauer, K. J. (1990) *Proc. Natl. Acad. Sci. USA* **87**, 9436–9440.
47. Broitman, S. J., Im, D. D. & Fresco, J. R. (1987) *Proc. Natl. Acad. Sci. USA* **84**, 5120–5124.
48. Chastain, M. & Tinoco, I., Jr. (1992) *Nucleic Acids Res.* **20**, 315–318.
49. Toulmé, J.-J. & Hélène, C. (1988) *Gene* **72**, 51–58.
50. Stein, C. A. & Cohen, J. S. (1988) *Cancer Res.* **48**, 2659–2668.
51. Kohlstaedt, L. A., Wang, J., Friedman, L. M., Rice, P. A. & Steitz, T. A. (1992) *Science* **256**, 1783–1790.
52. Sun, J.-S., François, J.-C., Montenay-Garestier, T., Saison-Behmoaras, T., Roig, V., Thuong, N. T. & Hélène, C. (1989) *Proc. Natl. Acad. Sci. USA* **86**, 9198–9202.